

FFT-based Dynamic Token Mixer for Vision

Yuki Tatsunami^{1,2} Masato Taki¹

¹Rikkyo University ²AnyTech Co., Ltd.

{y.tatsunami, taki_m}@rikkyo.ac.jp

Abstract

Multi-head-self-attention (MHSA)-equipped models have achieved notable performance in computer vision. Their computational complexity is proportional to quadratic numbers of pixels in input feature maps, resulting in slow processing, especially when dealing with high-resolution images. New types of token-mixer are proposed as an alternative to MHSA to circumvent this problem: an FFT-based token-mixer, similar to MHSA in global operation but with lower computational complexity. However, despite its attractive properties, the FFT-based token-mixer has not been carefully examined in terms of its compatibility with the rapidly evolving MetaFormer architecture. Here, we propose a novel token-mixer called dynamic filter and DFFormer and CDFFormer, image recognition models using dynamic filters to close the gaps above. CDFFormer achieved a Top-1 accuracy of 85.0%, close to the hybrid architecture with convolution and MHSA. Other wide-ranging experiments and analysis, including object detection and semantic segmentation, demonstrate that they are competitive with state-of-the-art architectures; Their throughput and memory efficiency when dealing with high-resolution image recognition is convolution and MHSA, not much different from ConvFormer, and far superior to CAFormer. Our results indicate that the dynamic filter is one of the token-mixer options that should be seriously considered. The code is available at <https://github.com/okojoalg/dfformer>

1. Introduction

A transformer architecture was propelled to the forefront of investigations in the computer vision field. The architecture locates the center in various visual recognition tasks, including not only image classification [16, 53, 67, 74, 58, 5] but also action recognition [37, 3], even point cloud understanding [18, 71, 60]. Vision Transformer (ViT) [16] and its variants triggered this explosion. ViT got inspired by Transformer in NLP and is equipped with a multi-head self-attention (MHSA) mechanism [56] as a critical ingre-

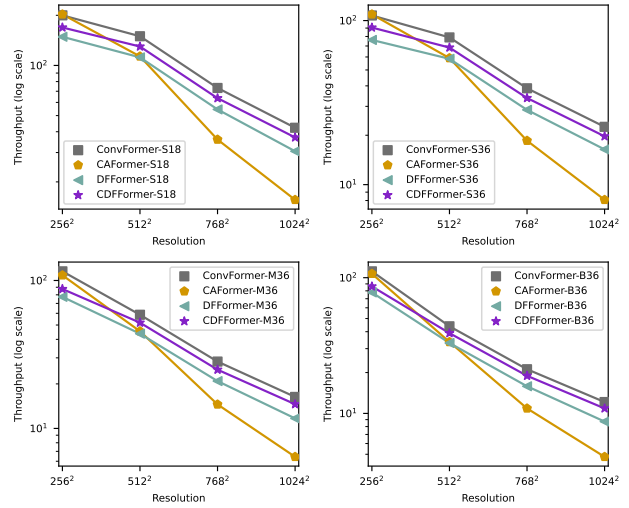


Figure 1: **Throughput vs. resolution.** Throughput has been benchmarked on a V100 with 16GB memory at a batch size of four.

dent. MHSA modules are low-pass filters [39]. Hence they suit for recognizing information about an entire image. While MHSA modules have been a success, it has faced challenges, especially in aspects of quadratic computational complexity due to global attention design. This problem is not agonizing in ImageNet classification but in dense tasks like semantic segmentation since we often deal with high-resolution input images. This problem can be tackled by using local attention design [33, 70, 10, 7], but the token-to-token interaction is limited, which means that one of the selling points of Transformers is mislaid.

GFNet [44] is one of the architectures induced by ViT and has two charming properties: (1) Global filter, the principal component in GFNet, multiplies features and complex parameters in frequency domains to increase/decrease a specific frequency. It is similar to a large kernel convolution [14, 32] but has the attractive aspect of reducing theoretical computational costs [44]. In addition, GFNet has less difficulty training than a large kernel convolution, whereas large kernel convolutions employ a tricky training

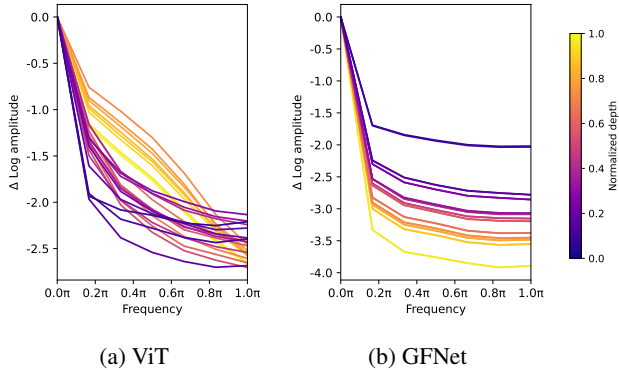


Figure 2: Relative log amplitudes of Fourier transformed feature maps. Δ Log amplitude means relative logarithmic amplitude concerning the logarithmic amplitude at normalized frequency 0. The yellower the color, the deeper the layer.

plan. Moreover, a computational complexity of GFNet is $\mathcal{O}(HWC[\log_2(HW)] + HWC')$, which is superior to of self-attention $\mathcal{O}(HWC^2 + (HW)^2C)$ where H is height, W is width, and C is channel. In other words, the higher the resolution of the input image, the more complexity GFNet has relative dominance. (2) A global filter is expected to serve as a low-pass filter like MHSA because global filter is a global operation with room to capture low-frequency information. We follow [39] and compare the relative log amplitudes of Fourier transformed between ViT, and GFNet, which is a non-hierarchical architecture similar to ViT, and show in Figure 2. The result demonstrates that GFNet retains the same low-frequency information nearby 0 as ViT. Thus, we need to address the potential for the global filter alternative to MHSA due to its computational advantage when handling high-resolution input images and its similarity to MHSA.

Global filters and MHSA are different in certain respects, even though have low-pass filter characteristics like they are different in certain respects. For example, MHSA is a data-dependent operation generated from data and applied to data. In contrast, global filters multiply data and parameters and hence are less data-dependent operations. In recent works, MLP-based models, which have been less data-dependent, employ data-dependent operations [59, 43], achieved accuracy improvements. It is inferred from the findings that introducing a data-dependent concept to global filters will improve accuracy.

Meanwhile, one should note that global filters have not been based on the most up-to-date and effective architectures relative to the well-researched MHSA-based and their relatives' architectures. MetaFormer [65, 66] pays attention to the overall architecture of the Transformer. MetaFormer has a main block consisting of a token-mixer which allows arbitrary and a channel mixer. It also makes see to consider this framework for global filters because it is one of

the most sophisticated architectures. It is necessary to close these differentials if global filters are effectively advanced as an alternative to MHSA modules and competitive accuracy is to be achieved.

We propose DFFormer, an FFT-based network, and CDDFormer, a hybrid architecture of convolutions and FFT-based modules, to fill the above gap. Our architectures inherit MetaFormer and equip modules that can dynamically generate a global filter for each pair of feature channels in the image, considering their contents. Our experimental results show that the proposed methods achieve state-of-the-art performance among vision models on the ImageNet-1K dataset, except for MHSA. In particular, CDDFormer-B36 with 113M parameters has achieved a top-1 accuracy of 85.0%. Moreover, when dealing with high-resolution images, the proposed method realizes higher throughput than the MHSA-based architecture and architecture using both CNN and MHSA. In addition, the proposed models are also adequate for dense prediction. We also found that the dynamic filter tends to learn low frequency rather than MHSA on a hierarchical Metaformer.

2. Related Work

Vision Transformers and Metaformers Transformer [56], which was proposed in NLP, has become a dominant architecture in computer vision as well, owing to the success of ViT [16] and DETR [6]. Soon after, MLP-Mixer [52] demonstrates that MLP can also proxy MHSA in Transformer. MetaFormer [65], as an abstract class of Transformer and MLP-Mixer, was proposed as a macro-architecture. The authors tested the hypothesis using MetaFormer with pooling. Generally, the abstract module corresponding to MHSA and MLP is called a token-mixer. It emphasizes the importance of MetaFormer that new classes MetaFormer, such as Sequencer [50] using RNNs and Vision GNN [20] using graph neural networks, emergent. Moreover, a follow-up study [66] has shown that even more highly accurate models can be developed by improving activation and hybridizing with multiple types of tokens. We retain the macro-architecture of [66]. In addition, FFT-based modules are characterized global operations like MHSA to achieve an efficient architecture for high-resolution images without much loss of accuracy.

FFT-based Networks In recent years, neural networks using Fourier transforms have been proposed. FNet [28], designed for NLP, contain modules using a discrete or fast Fourier Transform to extract only the real part. Accordingly, they have no parameters. Fast-FNet [45] removes waste and streamlines FNet. By contrast, GFNet [44] is an FFT-based network designed for vision with global filters. The global filter operates in frequency space by multiplying features with a Fourier filter, equivalent to a cyclic

convolution. The filter is a parameter, i.e., the same filter is used for all samples. Our dynamic filter can generate dynamically the Fourier filter using MLP. [17] is one of the most related works and has proposed AFNO. Instead of the element-wise product, the MLP operation of complex weights is used to represent an adaptive and non-separable convolution. AFNO is not a separable module. As a result, the computational cost is higher than the separable module. On the contrary, our proposed method can realize a dynamic separable Fourier filter, and our models do not differ much from the global filter in terms of FLOPs. We will mention these throughputs in subsection 4.4. Concurrent work [57] also attempts to generate dynamic filters, but the structure is such that only the filter coefficients are changed. Although the amplitude and frequency of the filter are dynamic, the major property of the filter cannot be changed (e.g., a high-pass filter cannot be changed to a low-pass filter). In contrast, a dynamic filter can represent high-pass and low-pass filters by first-order coupling.

Dynamic Weights There have been some suggestive studies on the generation of dynamic weights. [25] realizes the filter parameters to change dynamically, where the filter weights of the convolution were model parameters. A filter generation network generates the filters. [19] is a contemporaneous study. HyperNetworks it proposed are a neural network to create weights of another neural network. They can generate weights of CNN and RNN. [64, 9] are at the same time worked on, both of which make the filters of convolution dynamic. These works influence our dynamic filter: whereas [64, 9] predict the real coefficients of linear combination for a real filter basis of standard convolution, our work predicts the real coefficients of linear combination for a complex parameter filter basis. This method can be considered an equivalent operation in forward propagation from the fast Fourier transform’s linearity; thus, our work is similar to these works. In backpropagation, however, it is non-trivial whether the proposed dynamic filter can be learned. Our architecture does not also need the training difficulties cited in these studies, such as restrictions on batch size or adjustment of softmax temperatures. Outside of convolution, Synthesizer [51], DynaMixer [59], and AMixer [43] have MLP-Mixer-like token-mixer, but with dynamic generation of weights. In particular, AMixer includes linear combinations related to our work.

3. Method

3.1. Preliminary: Global Filter

We will look back at a discrete Fourier transform before introducing a global filter [44]. We discuss a 2D discrete Fourier transform (2D-DFT). For given the 2D signal

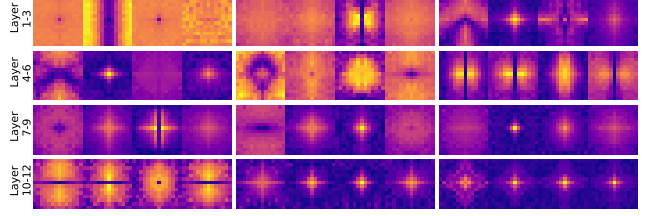


Figure 3: Filters in the frequency domain on GFNet-Ti

$x(h, w)$, we define the 2D-DFT $\tilde{x}(h', w')$ as following:

$$\tilde{x}(h', w') = \sum_{h=0}^{H-1} \sum_{w=0}^{W-1} \frac{x(h, w) e^{-2\pi j \left(\frac{h h'}{H} + \frac{w w'}{W} \right)}}{\sqrt{HW}} \quad (1)$$

where $H, W \in \mathbb{N}$, $h, h' \in \{z \in \mathbb{Z} | 0 < z < H\}$, and $w, w' \in \{z \in \mathbb{Z} | 0 < z < W\}$. Its inverse transformation exists and is well-known as a 2D inverse discrete Fourier transform (2D-IDFT). Generally, $\tilde{x}(h', w')$ is complex and periodic to h' and w' . We assume that $x(h', w')$ is a real number, then a complex matrix $\tilde{X}(h', w')$ associated with $\tilde{x}(h', w')$ is Hermitian. A space to which $\tilde{x}(h', w')$ belongs is known as a frequency domain and is available for analyzing frequencies. In addition, the frequency domain has a significant property: Multiplication in the frequency domain is equivalent to a cyclic convolution in the original domain, called convolution theorem [41]. The 2D-DFT is impressive but has a complexity of $\mathcal{O}(H^2 W^2)$. Therefore, a 2D-FFT is proposed and is often used in signal processing. It is improved with complexity $\mathcal{O}(HW \log_2(HW))$.

Second, we define the global filter for the feature $\mathbf{X} \in \mathbb{R}^{C \times H \times W}$. The global filter \mathcal{G} formulate the following:

$$\mathcal{G}(\mathbf{X}) = \mathcal{F}^{-1}(\mathbf{K} \odot \mathcal{F}(\mathbf{X})) \quad (2)$$

where \odot is the element-wise product, $\mathbf{K} \in \mathbb{C}^{C \times H \times \lceil \frac{W}{2} \rceil}$ is a learnable filter, and \mathcal{F} is the 2D-FFT of which redundant components are reduced (i.e., $\text{rfft}2$) since $\mathcal{F}(x)$ is Hermitian. Note that the operation is equivalent to cyclic convolution of the filter $\mathcal{F}^{-1}(\mathbf{K})$ based on the convolution theorem.

The global filter is known to have some properties. (1) The theoretical complexity is $\mathcal{O}(HWC[\log_2(HW)] + HWC)$. It is more favorable than Transformer and MLP when input is high resolution. (2) The global filter can easily scale up the input resolution owing to interpolating the filter. See [44] for more details.

3.2. Dynamic Filter

This subsection discusses a dynamic filter in which a neural network dynamically determines an adequate global filter. Figure 4a show the dynamic filter, has global filter basis of which the dimension is N , and linearly coupled global

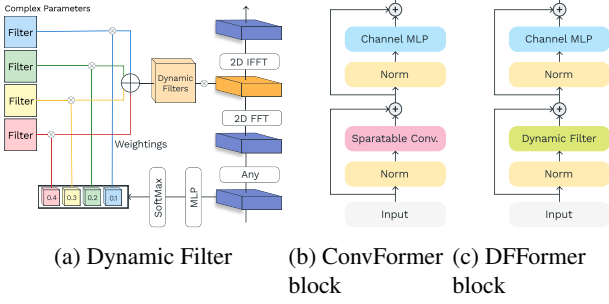


Figure 4: **(a) Dynamic Filter.** "Any" modules are allowed continuous real maps. **(b) ConvFormer block** proposed by [66]. **(c) DFFormer block** is MetaFormer block, equipped with the dynamic filter.

filters for them are used for each channel instead of learnable global filters. The coefficients are ruled by an MLP \mathcal{M} . We specify the whole dynamic filter \mathcal{D} as follows:

$$\mathcal{D}(\mathbf{X}) = \mathcal{F}^{-1}(\mathcal{K}_{\mathcal{M}}(\mathbf{X}) \odot \mathcal{F} \circ \mathcal{A}(\mathbf{X})) \quad (3)$$

where $\mathcal{K}_{\mathcal{M}}$ denotes the function that determines the dynamic filter. \mathcal{A} are continuous real maps, including point-wise convolutions and identity maps.

Generating Dynamic Filter We denote global filter basis \mathbb{K} so that $\mathbb{K} = \{\mathcal{K}_1, \dots, \mathcal{K}_N\}$ and $\mathcal{K}_1, \dots, \mathcal{K}_N \in \mathbb{C}^{H \times \lceil \frac{W}{2} \rceil}$. Filters $\mathcal{K}_{\mathcal{M}}(\mathbf{X}) \in \mathbb{C}^{C' \times H \times \lceil \frac{W}{2} \rceil}$ are associated with \mathcal{M} for weighting and are defined by the following:

$$\mathcal{K}_{\mathcal{M}}(\mathbf{X})_{c,:,:} := \sum_{i=1}^N \left(\frac{e^{s(c-1)N+i}}{\sum_{n=1}^N e^{s(c-1)N+n}} \right) \mathcal{K}_i, \quad (4)$$

$$\text{where } (s_1, \dots, s_{NC'})^\top = \mathcal{M} \left(\frac{\sum_{h,w} \mathbf{X}_{:,h,w}}{HW} \right). \quad (5)$$

In this paper, we use $N = 4$, which is the dimension of \mathbb{K} , to avoid over-computing. See ablation in subsection 4.4.

MLP for weighting We describe MLP \mathcal{M} for weighting throughout specific calculation formulas:

$$\mathcal{M}(\mathbf{X}) = W_2 \text{StarReLU}(W_1 \text{LN}(\mathbf{X})), \quad (6)$$

where $\text{LN}(\cdot)$ is layer normalization [1], $\text{StarReLU}(\cdot)$ is an activation function proposed by [66], $W_1 \in \mathbb{R}^{C \times \text{int}(\rho C)}$, $W_2 \in \mathbb{R}^{\text{int}(\rho C) \times NC'}$ denote matrices of MLP layer, ρ is a ratio of the intermediate dimension to the input dimension of MLP. We choose $\rho = 0.25$ but see section 4.4 for the other case.

3.3. DFFormer and CDFFormer

We construct DFFormer and CDFFormer complying with MetaFormer [66]. DFFormer and CDFFormer mainly

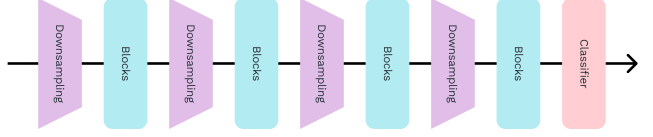


Figure 5: A four-stage model

Model	DFFormer	CDFFormer
Token Mixer	(DF, DF, DF, DF)	(CF, CF, DF, DF)
Down Sampling	$K = (7, 3, 3, 3), S = (4, 2, 2, 2), P = (2, 1, 1, 1)$	
Size	S18	$L = (3, 3, 9, 3), C = (64, 128, 320, 512)$
	S36	$L = (3, 3, 9, 3), C = (64, 128, 320, 512)$
	M36	$L = (3, 3, 9, 3), C = (96, 192, 384, 576)$
	B36	$L = (3, 3, 9, 3), C = (128, 256, 512, 768)$
Classifier	Global average pooling, Layer Norm., MLP	

Table 1: **Model settings of DFFormer and CDFFormer.** DF and CF mean DFFormer block and CFFormer block, respectively. K, S, P, C , and L denote kernel size, stride, padding, number of channels, and number of blocks, respectively. The indices of each tuple correspond to the order of the stages.

consist of MetaFormer blocks, such as DFFormer blocks and ConvFormer blocks. DFFormer and CDFFormer blocks comply with MetaFormer blocks

$$\mathcal{T}(\mathbf{X}) = \mathbf{X} + \text{Conv}_{\text{pw}2} \circ \mathcal{L} \circ \text{StarReLU} \circ \text{Conv}_{\text{pw}1} \circ \text{LN}(\mathbf{X}) \quad (7)$$

where $\text{LN}(\cdot)$ is Layer Normalization [1], $\text{Conv}_{\text{pw}1}(\cdot)$ and $\text{Conv}_{\text{pw}2}(\cdot)$ are point-wise convolutions so that the number of output channels is $(C' =) 2C$ and C , respectively, and $\mathcal{L}(\cdot)$ is dimensional invariant any function. If $\mathcal{L}(\cdot)$ is separable convolution, \mathcal{T} is named as ConvFormer block at [66]. If $\mathcal{L}(\cdot) = \mathcal{F}^{-1}(\mathcal{K}_{\mathcal{M}}(\mathbf{X}) \odot \mathcal{F}(\cdot))$, we define that \mathcal{T} is DF-Former block. A schematic diagram is shown in Figure 4b and 4c in order to understand these blocks' structure. See codes for details in the appendix.

The overall framework is also following MetaFormer [65, 66]. In other words, we utilize the four-stage model in Figure 5. We prepared four sizes of models for DF-Former, which mainly consists of DFFormer blocks, and CDFFormer, which is a hybrid model of DFFormer blocks and ConvFormer blocks. Each model equips with an MLP classifier with Squared ReLU [47] as the activation. A detailed model structure is shown in Table 1.

4. Experiments

We conduct experiments on ImageNet-1K benchmark [27] and perform further experiments to confirm downstream tasks such as COCO benchmark [31] and ADE20K [73]. Finally, we compare state-of-the-art in the past and conduct ablation studies about design elements.

Model	Family	Params (M)	FLOPs (G)	Thr. (im/s)	Top-1 (%)
ResNet-50 [21, 62]	Conv	26	4.1	1672	79.8
ConvNeXt-T [34]	Conv	29	4.5	1471	82.1
ConvFormer-S18 [66]	Conv	27	3.9	756	83.0
DeiT-S [53]	Attn	22	4.6	1513	79.8
CSWin-T [15]	Attn	23	4.3	340	82.7
MViTv2-T [29]	Attn	24	4.7	624	82.3
AMixer-T [43]	MLP	26	4.5	724	82.0
GFNet-H-S [44]	FFT	32	4.6	952	81.5
DFFormer-S18	FFT	30	3.8	535	83.2
CoAtNet-0 [13]	Conv + Attn	25	4.2	1238	81.6
CAFormer-S18 [66]	Conv + Attn	26	4.1	741	83.6
CDFFormer-S18	Conv + FFT	30	3.9	567	83.1
ResNet-101 [21, 62]	Conv	45	7.9	859	81.3
ConvNeXt-S [34]	Conv	50	8.7	864	83.1
ConvFormer-S36 [66]	Conv	40	7.6	398	84.1
CSWin-S [15]	Attn	35	6.9	218	83.6
MViTv2-S [29]	Attn	35	7.0	416	83.6
DynaMixer-S [59]	MLP	26	7.3	448	82.7
AMixer-S [43]	MLP	46	9.0	378	83.5
GFNet-H-B [44]	FFT	54	8.6	612	82.9
DFFormer-S36	FFT	46	7.4	270	84.3
CoAtNet-1 [13]	Conv + Attn	42	8.4	591	83.3
CAFormer-S36 [66]	Conv + Attn	39	8.0	382	84.5
CDFFormer-S36	Conv + FFT	45	7.5	319	84.2
ResNet-152 [21, 62]	Conv	60	11.6	610	81.8
ConvNeXt-B [34]	Conv	89	15.4	687	83.8
ConvFormer-M36 [66]	Conv	57	12.8	307	84.5
DeiT-B [53]	Attn	86	17.5	887	81.8
CSWin-B [15]	Attn	78	15.0	217	84.2
MViTv2-B [29]	Attn	52	10.2	285	84.4
DynaMixer-M [59]	MLP	57	17.0	317	83.7
AMixer-B [43]	MLP	83	16.0	325	84.0
DFFormer-M36	FFT	65	12.5	210	84.6
CoAtNet-2 [13]	Conv + Attn	75	15.7	582	84.1
CAFormer-M36 [66]	Conv + Attn	56	13.2	297	85.2
CDFFormer-M36	Conv + FFT	64	12.7	254	84.8
RegNetY-32G [42, 62]	Conv	145	32.3	415	82.4
ConvNeXt-L [34]	Conv	198	34.4	431	84.3
ConvFormer-B36 [66]	Conv	100	22.6	235	84.8
MViTv2-L [29]	Attn	218	42.1	128	85.3
DynaMixer-L [59]	MLP	97	27.4	216	84.3
DFFormer-B36	FFT	115	22.1	161	84.8
CoAtNet-3 [13]	Conv + Attn	168	34.7	439	84.5
CAFormer-B36 [66]	Conv + Attn	99	23.2	227	85.5
CDFFormer-B36	Conv + FFT	113	22.5	195	85.0

Table 2: **Performance comparison of models pre-trained on ImageNet-1K at the resolution of 224².** Throughput has been benchmarked on a V100 with 16GB memory at a batch size of 16.

4.1. Image Classification

DFFormers and CDFFormers have experimented on ImageNet-1K [27], one of the most renowned data sets in

Backbone	Params (M)	AP (%)	AP ₅₀ (%)	AP ₇₅ (%)	AP _S (%)	AP _M (%)	AP _L (%)
ResNet-50 [21]	37.7	36.3	55.3	38.6	19.3	40.0	48.8
PoolFormer-S24 [65]	31.1	38.9	59.7	41.3	23.3	42.1	51.8
DFFormer-S18	38.1	43.6	64.5	46.6	27.5	47.3	58.1
CDFFormer-S18	37.4	43.4	64.7	46.3	26.3	47.1	57.3
ResNet-101 [21]	56.7	38.5	57.8	41.2	21.4	42.6	51.1
PoolFormer-S36 [65]	40.6	39.5	60.5	41.8	22.5	42.9	52.4
DFFormer-S36	53.8	45.3	66.1	48.7	26.9	49.0	59.9
CDFFormer-S36	52.6	45.0	66.0	47.8	27.6	48.5	59.6

Table 3: **Performance comparison of models using RetinaNet trained on COCO.** The settings follow [65] and the compared model’s results are cited from [65].

computer vision for image classification. It has 1000 classes and contains 1,281,167 training images and 50,000 validation images. Our training strategy is mainly according to [53] and is detailed as follows. For data augmentation methods, we apply MixUp [69], CutMix [68], random erasing [72], and RandAugment [12]. Stochastic depth [24] and label smoothing [49] are used to regularize. We employ AdamW [35] optimizer for 300 epochs with a batch size of 1024. The base learning rate of $\frac{\text{batch size}}{512} \times 5 \times 10^{-4}$, 20 epochs of linear warm-up, cosine decay for learning rate, and weight decay of 0.05 are used. The implementation is based on PyTorch [40] and timm [61]. The details of the hyperparameters are presented in the appendix.

We compare the proposed models with state-of-the-art models, including CNN-based, attention-based, MLP-based, FFT-based, and hybrid models. Table 2 shows the results. We can see that DFFormers and CDFFormers perform impressive top-1 accuracy among models except for CAFormers with comparable parameters. In other words, DFFormer and CDFFormer can have a performance that is next to CAFormer. Primarily, DFFormers perform more than 0.5% better than other FFT-based models and have been ahead of MLP-based models[43, 59], to which FFT-based tends to compare. The above performance comparison of DFFormer and CDFFormer indicates that dynamic filters are promising modules for image recognition.

4.2. Object Detection on COCO

We evaluate our models’ performance on downstream tasks, especially in object detection on COCO benchmark [31]. It has 80 classes consisting of 118,287 training images and 5,000 validation images. We employ RetinaNet as an object detection framework. The implementation takes [30] of mmdet [8]. We utilize pre-trained models on ImageNet-1K dataset as the backbones. Following the setting in [65], we use $1 \times$ training, meaning 12 epochs, batch size of 16, and AdamW [35] optimizer with an initial learning rate of 10^{-4} . Similar to the general setup, training images of coco

Backbone	Params (M)	mIoU (%)
ResNet-50 [21]	28.5	36.7
PVT-Small [58]	28.2	39.8
PoolFormer-S24 [65]	23.2	40.3
DFFormer-S18	31.7	45.1
CDFFormer-S18	31.4	44.9
ResNet-101 [21]	47.5	38.8
ResNeXt-101-32x4d [63]	47.1	39.7
PVT-Medium [58]	48.0	41.6
PoolFormer-S36 [65]	34.6	42.0
DFFormer-S36	47.2	47.5
CDFFormer-S36	46.5	46.7
PVT-Large [58]	65.1	42.1
PoolFormer-M36 [65]	59.8	42.4
DFFormer-M36	66.4	47.6
CDFFormer-M36	65.2	48.6

Table 4: **Performance comparison of models using Semantic FPN trained on ADE20K.** The settings follow [65] and the compared model’s results are cited from [65].

are resized to no more than 800 pixels on the short side and 1,333 pixels on the long side, keeping the aspect ratio. The testing images are also resized to 800 pixels on the short side. The default dynamic filter does not support arbitrary resolutions because of using the element-wise product. Although input images have an indeterminate resolution in the setting, pre-trained DFFormer and CDFFormer are bound with the resolution of 224^2 . To cancel this problem, we bicubic interpolate global filter basis \mathbb{K} so that fit images with a resolution of 800^2 and let it be new parameters. Moreover, the global filter basis is interpolated to adjust to the shape of frequency features which is input to dynamic filters.

Table 3 shows RetinaNets with DFFormer and CDFFormer as backbone outperform comparable ResNet and PoolFormer backbones. For instance, DFFormer-S36 has 5.8 points higher AP than PoolFormer-S36. Thus, DFFormer and CDFFormer obtained competitive results in COCO object detection.

4.3. Semantic Segmentation on ADE20K

We train and test our models on ADE20K [73] dataset for a semantic segmentation task to evaluate the performance in dense prediction tasks. It has 150 semantic categories, 20,210 images for training, 2,000 for validation, and 3,000 for testing. We employ Semantic FPN [26] in mmseg [11] as a base framework. Training images are resized and cropped to a shape of 512^2 . For testing, images are resized to a shorter size of 512 pixels, keeping the aspect ratio. We adopt global filter basis parameters \mathbb{K} interpolated from pre-trained parameters to suit images with a resolution of 512^2 . For testing, \mathbb{K} is also interpolated for the same reason as subsection 4.2. We utilize AdamW [35] optimizer,

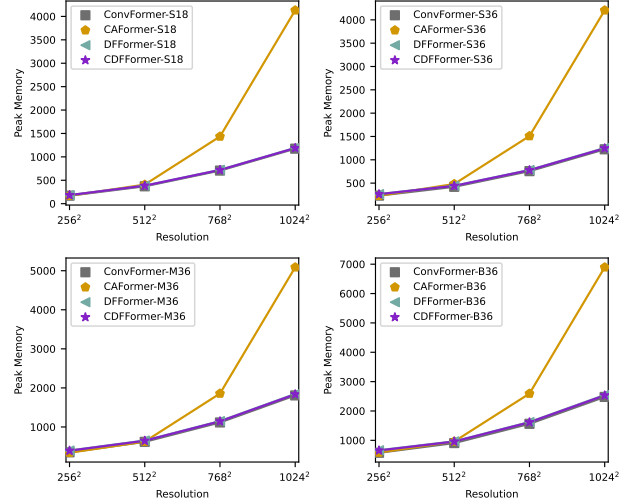


Figure 6: **Peak memory vs. resolution.** Peak memory has been benchmarked on a V100 with 16GB memory at a batch size of four.

initial learning rate of 2×10^{-4} , polynomial scheduler with a power 0.9, batch size of 32, and 40K iterations, following [65].

Table 4 shows that DFFormer-based and CDFFormer-based models equipped with Semantic FPN for semantic segmentation are effective for the semantic segmentation task. They are superior to those based on other models, including PoolFormer-based models. From these results, it can be seen that DFFormer-S36 has 5.5 points higher mIoU than PoolFormer-S36. In addition, CDFFormer-M36 achieves 48.6 mIoU. As a result, we also verify the effectiveness of DFFormer and CDFFormer for semantic segmentation.

4.4. Ablation Studies

We experiment with ablation studies on the ImageNet-1K dataset. Let us discuss ablation from several perspectives.

Filter We studied how changing filters would work. First, we change to the hyperparameters of dynamic filters. Specifically, we train and test models in which the dimension of dynamic filter base N and the intermediate dimension ρC are modified in half of the cases, respectively. From Table 5, however, we found that the throughput and number of parameters remained almost the same, and the accuracy dropped by 0.2% and 0.1%, respectively. Next, we train GFFormer-S18, which is replaced by the dynamic filter of DFFormer-S18 with a global filter (i.e., static filter) to confirm the effectiveness of dynamic filters. Table 5 demonstrates DFFormer-S18 is superior to GFFormer-S18 0.3%. We also have studied a case where AFNOs replaced

Ablation	Variant	Params (M)	FLOPs (G)	Thr. (im/s)	Top-1 (%)
Baseline	DFFormer-S18	30	3.8	535	83.2
	$N = 4 \rightarrow 2$	29	3.8	534	83.0
Filter	$\rho = 0.25 \rightarrow 0.125$	28	3.8	532	83.1
	GFFormer-S18 (Dynamic Filter \rightarrow Global Filter [44])	30	3.8	575	82.9
	Dynamic Filter \rightarrow AFNO [17]	30	3.8	389	82.6
Activation	StarReLU [66] \rightarrow GELU [22]	30	3.8	672	82.7
	StarReLU [66] \rightarrow ReLU [36]	30	3.8	640	82.5

Table 5: Ablation for DFFormer-S18 on ImageNet-1K. Remind N is the dimension of the dynamic filter basis, and ρ is a ratio of MLP intermediate dimension to input dimension.

dynamic filters but found that the AFNO-based model degraded in accuracy more than the dynamic filter and that dynamic filters are better throughput than AFNOs.

Activation DFFormer and CDDFormer use StarReLU, but this is a relatively new activation; many MetaFormers employ Gaussian Error Linear Unit (GELU) [22], and earlier generations of convolutional neural networks (CNNs), such as ResNet [21], often used Rectified Linear Unit (ReLU) [36]. Accordingly, we also experiment with a version of the model in which GELU and ReLU replace StarReLU in DFFormer-S18. As a result, Table 5 shows that DFFormer-S18 outperforms the replaced version of the model by more than 0.5%, demonstrating that StarReLU is also a valuable activation for dynamic filters.

5. Analysis

5.1. Advantages at Higher Resolutions

We observe how the throughput at inference and peak memory change on proposed and comparative models when the resolution varies. For throughput, the proposed models have been inferior to CAFormer, an architecture that utilized MHSA, at a resolution of 224^2 since Table 2 can comprehend the fact. The result conflicts with the computational complexity presented in the Introduction. Our interpretation of the issue is that the actual throughput would depend on the implementation of FFT (although we use `cuFFT` via `PyTorch`), hardware design, etc. Increasing the resolution, the theoretically computational complexity of MHSA comes into effect: Figure 1 shows the throughput for different resolutions. DFFormer and CDDFormer maintain throughput close to that of ConvFormer, while only CAFormer shows a significant decrease in throughput. The same is true for peak memory in Figure 6: Whereas the CAFormer peak memory increases, the DFFormer and CDDFormer peak memory is comparable to that of ConvFormer. Therefore, DFFormer and CDDFormer are beneficial in speed- and memory-constrained environments for tasks such as semantic segmentation, where high resolution

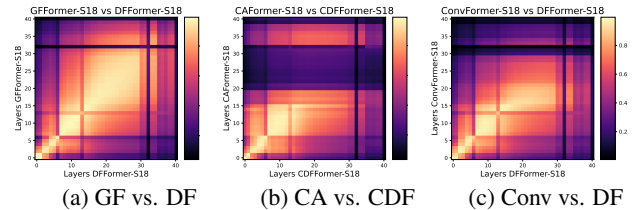


Figure 7: The feature map similarities by CKA

is required.

5.2. Representational Similarities

Figure 7 shows the similarities between GFFormer-S18 and DFFormer-S18, ConvFormer-S18 and DFFormer-S18, and CAFormer-S18 and CDDFormer-S18 in the validation set of ImageNet-1K. In our analysis, we metric the similarity using mini-batch linear CKA [38]. `torch_cka` [48] toolbox was used to implement the mini-batch linear CKA. The layers to be analyzed included four downsampled and 18 token-mixers residual blocks and 18 channel MLP residual blocks, and the indices in the figure are ordered from the shallowest layer. Figure 7a shows that GFFormer-S18 and DFFormer-S18 are very similar up to stage 3, although they are slightly different at stage 4. We also found the same thing about the similarity between ConvFormer-S18 and DFFormer-S18 from Figure 7c. On the contrary, Figure 7b shows that CAFormer-S18 and CDDFormer-S18 are similar up to stage 2 with convolution but become almost entirely different from stage 3 onward. Even though FFT-based token-mixers, like MHSA, are token-mixers in the global domain and can capture low-frequency features, they necessarily do not learn similar representations. The fact would hint that MHSA and the FFT-based token-mixer have differences other than spatial mixing. We perform a Fourier analysis on stage 3 to know the difference in stage 3. Figure 8 shows the difference between MHSA and FFT-based token-mixer results. Surprisingly, CAFormer-S18 acts as a high-path filter, whereas CDDFormer-S18 indicates to be more attenuated at other frequencies other than around 0. In other words, MHSA incorporated in a hierarchical archi-

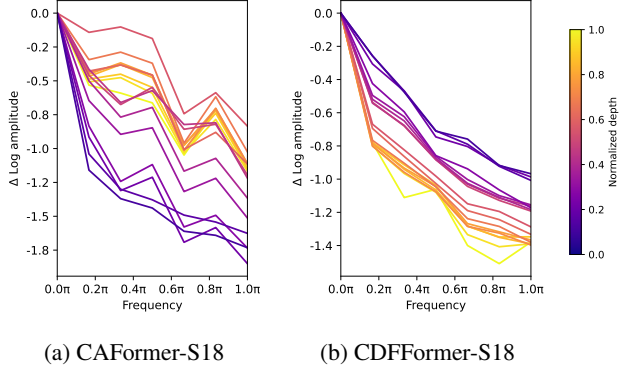


Figure 8: Relative log amplitudes of Fourier transformed feature maps on stage 3. A setup similar to that in Table 2.

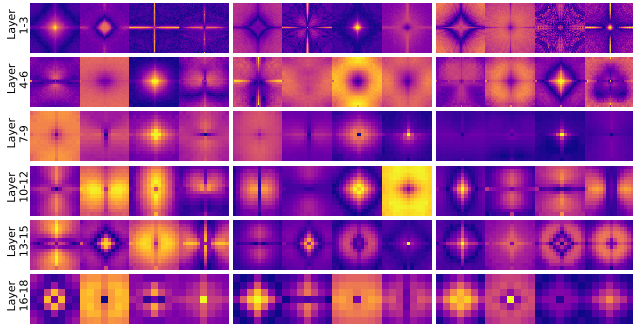


Figure 9: Filters in the frequency domain on DFFormer-S18

texture can learn high-path and low-path filters while the dynamic filter attenuates the high frequencies. Only applying to stage 3 makes the analysis more interpretable than overall because this analysis drastically changes frequency by downsampling.

5.3. Analysis of Dynamic Filter Basis

The basis of complex parameters in the frequency domain can represent dynamic filters used in DFFormer and CDFFormer. Here, we visualize them for DFFormer-S18, which has four in each dynamic filter module. The frequency 0 is taken as the center in our visualization, and the yellower pixel means higher amplitudes. Figure 9 demonstrates that the redundancy of filters in the same layer is reduced compared to Figure 3 about GFNet-Ti. In addition, we can see high-pass, low-pass, and band-pass filters in many layers. Details of the visualization method and more visualization will be given in the appendix.

5.4. Global and Dynamic Filters Have a More Human-like Shape Bias

We found that the CNN+FFT-based and FFT-based models have shape bias compared to the baseline CNN+MHSA-

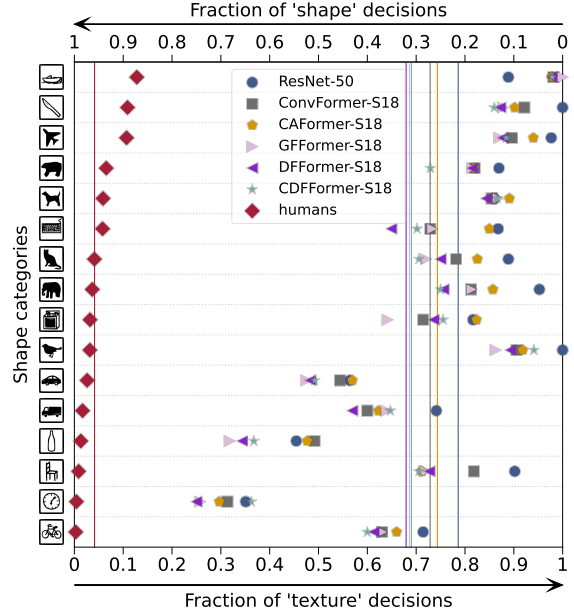


Figure 10: S18 models vs human on shape bias

based and CNN-based. We compare three models, DFFormer-S18, CDFFormer-S18, and GFFormer-S18, with baseline ResNet-50, ConvFormer-S18, CAFormer-S18, and humans where each model is pre-trained on ImageNet-1K. We use a toolbox [4] to evaluate shape or texture bias trends. The toolbox enables quickly following the setup of the previous studies that have used various out-of-distribution data to evaluate and, based on them, determine whether they tend toward shape or texture bias. Figure 10 proves that models with FFTs have shape bias compared to other models. Furthermore, it is interesting to note that the only difference in comparing MetaFormer models is the token-mixer. Hence, choosing an FFT-based token-mixer gives model criteria biased toward the shape.

6. Conclusion

This paper studied the similarities and differences between the global filter and MHSA in vision models. According to the analysis, we proposed a novel dynamic filter responsible for dynamically generating global filters. Based on this module, we have developed new MetaFormer classes, DFFormer and CDFFormer, which achieve performance outperforming the state-of-the-art MHSA-free MetaFormers. We have proven through a variety of experiments that the proposed models perform impressively not only in image classification but also in downstream tasks. In addition, our models can process high-resolution images faster and with less memory than MetaFormers using MHSA. We also found that the representation and properties of our models are not similar unexpectedly to that of models using MHSA.

Acknowledgement

- AI Bridging Cloud Infrastructure (ABCI) from Advanced Industrial Science and Technology (AIST) was used for the present work.
- The present work was supported by Rikkyo SFR (graduate student research package type: No.10).

References

- [1] Jimmy Lei Ba, Jamie Ryan Kiros, and Geoffrey E Hinton. Layer normalization. In *NeurIPS*, 2016.
- [2] Nicholas Baker, Hongjing Lu, Gennady Erlikhman, and Philip J Kellman. Deep convolutional networks do not classify based on global object shape. *PLoS computational biology*, 14(12):e1006613, 2018.
- [3] Gedas Bertasius, Heng Wang, and Lorenzo Torresani. Is space-time attention all you need for video understanding? In *ICML*, 2021.
- [4] bethgelab. Toolbox of model-vs-human. <https://github.com/bethgelab/model-vs-human>, 2022.
- [5] Lucas Beyer, Pavel Izmailov, Alexander Kolesnikov, Mathilde Caron, Simon Kornblith, Xiaohua Zhai, Matthias Minderer, Michael Tschannen, Ibrahim Alabdulmohsin, and Filip Pavetic. Flexivit: One model for all patch sizes. *arXiv preprint arXiv:2212.08013*, 2022.
- [6] Nicolas Carion, Francisco Massa, Gabriel Synnaeve, Nicolas Usunier, Alexander Kirillov, and Sergey Zagoruyko. End-to-end object detection with transformers. In *ECCV*, pages 213–229. Springer, 2020.
- [7] Chun-Fu Chen, Rameswar Panda, and Quanfu Fan. Regionvit: Regional-to-local attention for vision transformers. In *ICLR*, 2022.
- [8] Kai Chen, Jiaqi Wang, Jiangmiao Pang, Yuhang Cao, Yu Xiong, Xiaoxiao Li, Shuyang Sun, Wansen Feng, Ziwei Liu, Jiarui Xu, Zheng Zhang, Dazhi Cheng, Chenchen Zhu, Tianheng Cheng, Qijie Zhao, Buyu Li, Xin Lu, Rui Zhu, Yue Wu, Jifeng Dai, Jingdong Wang, Jianping Shi, Wanli Ouyang, Chen Change Loy, and Dahua Lin. MMDetection: Open mmlab detection toolbox and benchmark. *arXiv preprint arXiv:1906.07155*, 2019.
- [9] Yinpeng Chen, Xiyang Dai, Mengchen Liu, Dongdong Chen, Lu Yuan, and Zicheng Liu. Dynamic convolution: Attention over convolution kernels. In *CVPR*, pages 11030–11039, 2020.
- [10] Xiangxiang Chu, Zhi Tian, Yuqing Wang, Bo Zhang, Haibing Ren, Xiaolin Wei, Huaxia Xia, and Chunhua Shen. Twins: Revisiting the design of spatial attention in vision transformers. *Advances in Neural Information Processing Systems*, 34:9355–9366, 2021.
- [11] MMSegmentation Contributors. MMSegmentation: Openmmlab semantic segmentation toolbox and benchmark. <https://github.com/open-mmlab/mms Segmentation>, 2020.
- [12] Ekin D Cubuk, Barret Zoph, Jonathon Shlens, and Quoc V Le. RandAugment: Practical automated data augmentation with a reduced search space. In *CVPRW*, pages 702–703, 2020.
- [13] Zihang Dai, Hanxiao Liu, Quoc V Le, and Mingxing Tan. Coatnet: Marrying convolution and attention for all data sizes. In *NeurIPS*, volume 34, pages 3965–3977, 2021.
- [14] Xiaohan Ding, Xiangyu Zhang, Yizhuang Zhou, Jungong Han, Guiguang Ding, and Jian Sun. Scaling up your kernels to 31x31: Revisiting large kernel design in cnns. In *CVPR*, 2022.
- [15] Xiaoyi Dong, Jianmin Bao, Dongdong Chen, Weiming Zhang, Nenghai Yu, Lu Yuan, Dong Chen, and Baining Guo. Cswin transformer: A general vision transformer backbone with cross-shaped windows. In *CVPR*, 2022.
- [16] Alexey Dosovitskiy, Lucas Beyer, Alexander Kolesnikov, Dirk Weissenborn, Xiaohua Zhai, Thomas Unterthiner, Mostafa Dehghani, Matthias Minderer, Georg Heigold, Sylvain Gelly, et al. An image is worth 16x16 words: Transformers for image recognition at scale. In *ICLR*, 2021.
- [17] John Guibas, Morteza Mardani, Zongyi Li, Andrew Tao, Anima Anandkumar, and Bryan Catanzaro. Adaptive fourier neural operators: Efficient token mixers for transformers. In *ICLR*, 2022.
- [18] Meng-Hao Guo, Jun-Xiong Cai, Zheng-Ning Liu, Tai-Jiang Mu, Ralph R Martin, and Shi-Min Hu. Pct: Point cloud transformer. *Computational Visual Media*, 7(2):187–199, 2021.
- [19] David Ha, Andrew Dai, and Quoc V Le. Hypernetworks. In *ICLR*, 2016.
- [20] Kai Han, Yunhe Wang, Jianyuan Guo, Yehui Tang, and Enhua Wu. Vision gnn: An image is worth graph of nodes. In *NeurIPS*, 2022.
- [21] Kaiming He, Xiangyu Zhang, Shaoqing Ren, and Jian Sun. Deep residual learning for image recognition. In *CVPR*, pages 770–778, 2016.
- [22] Dan Hendrycks and Kevin Gimpel. Gaussian error linear units (GELUs). *arXiv preprint arXiv:1606.08415*, 2016.
- [23] Katherine Hermann, Ting Chen, and Simon Kornblith. The origins and prevalence of texture bias in convolutional neural networks. In *NeurIPS*, volume 33, pages 19000–19015, 2020.
- [24] Gao Huang, Yu Sun, Zhuang Liu, Daniel Sedra, and Kilian Q Weinberger. Deep networks with stochastic depth. In *ECCV*, pages 646–661, 2016.
- [25] Xu Jia, Bert De Brabandere, Tinne Tuytelaars, and Luc V Gool. Dynamic filter networks. In *NeurIPS*, volume 29, 2016.
- [26] Alexander Kirillov, Ross Girshick, Kaiming He, and Piotr Dollár. Panoptic feature pyramid networks. In *CVPR*, pages 6399–6408, 2019.
- [27] Alex Krizhevsky, Ilya Sutskever, and Geoffrey E Hinton. Imagenet classification with deep convolutional neural networks. In *NeurIPS*, volume 25, pages 1097–1105, 2012.
- [28] James Lee-Thorp, Joshua Ainslie, Ilya Eckstein, and Santiago Ontanon. Fnet: Mixing tokens with fourier transforms. In *NAACL*, 2022.
- [29] Yanghao Li, Chao-Yuan Wu, Haoqi Fan, Kartikeya Mangalam, Bo Xiong, Jitendra Malik, and Christoph Feichtenhofer. Mvitv2: Improved multiscale vision transformers for classification and detection. In *CVPR*, pages 4804–4814, 2022.

- [30] Tsung-Yi Lin, Priya Goyal, Ross Girshick, Kaiming He, and Piotr Dollár. Focal loss for dense object detection. In *ICCV*, pages 2980–2988, 2017.
- [31] Tsung-Yi Lin, Michael Maire, Serge Belongie, James Hays, Pietro Perona, Deva Ramanan, Piotr Dollár, and C Lawrence Zitnick. Microsoft coco: Common objects in context. In *ECCV*, pages 740–755, 2014.
- [32] Shiwei Liu, Tianlong Chen, Xiaohan Chen, Xuxi Chen, Qiao Xiao, Boqian Wu, Mykola Pechenizkiy, Decebal Mocanu, and Zhangyang Wang. More convnets in the 2020s: Scaling up kernels beyond 51x51 using sparsity. In *ICLR*, 2023.
- [33] Ze Liu, Yutong Lin, Yue Cao, Han Hu, Yixuan Wei, Zheng Zhang, Stephen Lin, and Baining Guo. Swin transformer: Hierarchical vision transformer using shifted windows. In *ICCV*, 2021.
- [34] Zhuang Liu, Hanzi Mao, Chao-Yuan Wu, Christoph Feichtenhofer, Trevor Darrell, and Saining Xie. A convnet for the 2020s. In *CVPR*, 2022.
- [35] Ilya Loshchilov and Frank Hutter. Decoupled weight decay regularization. In *ICLR*, 2019.
- [36] Vinod Nair and Geoffrey E Hinton. Rectified linear units improve restricted boltzmann machines. In *ICML*, 2010.
- [37] Daniel Neimark, Omri Bar, Maya Zohar, and Dotan Asselmann. Video transformer network. In *ICCV*, pages 3163–3172, 2021.
- [38] Thao Nguyen, Maithra Raghu, and Simon Kornblith. Do wide and deep networks learn the same things? uncovering how neural network representations vary with width and depth. In *ICLR*, 2021.
- [39] Namuk Park and Songkuk Kim. How do vision transformers work? In *ICLR*, 2022.
- [40] Adam Paszke, Sam Gross, Francisco Massa, Adam Lerer, James Bradbury, Gregory Chanan, Trevor Killeen, Zeming Lin, Natalia Gimelshein, Luca Antiga, et al. Pytorch: An imperative style, high-performance deep learning library. In *NeurIPS*, volume 32, 2019.
- [41] John G Proakis. *Digital signal processing: principles, algorithms, and applications, 4/E*. Pearson Education India, 2007.
- [42] Ilija Radosavovic, Raj Prateek Kosaraju, Ross Girshick, Kaiming He, and Piotr Dollár. Designing network design spaces. In *CVPR*, pages 10428–10436, 2020.
- [43] Yongming Rao, Wenliang Zhao, Jie Zhou, and Jiwen Lu. Amixer: Adaptive weight mixing for self-attention free vision transformers. In *ECCV*, pages 50–67. Springer, 2022.
- [44] Yongming Rao, Wenliang Zhao, Zheng Zhu, Jiwen Lu, and Jie Zhou. Global filter networks for image classification. In *NeurIPS*, volume 34, 2021.
- [45] Nurullah Sevim, Ege Ozan Özyedek, Furkan Şahinuş, and Aykut Koç. Fast-fnet: Accelerating transformer encoder models via efficient fourier layers. *arXiv preprint arXiv:2209.12816*, 2022.
- [46] Sam Shleifer, Jason Weston, and Myle Ott. Normformer: Improved transformer pretraining with extra normalization. *arXiv preprint arXiv:2110.09456*, 2021.
- [47] David R So, Wojciech Mańke, Hanxiao Liu, Zihang Dai, Noam Shazeer, and Quoc V Le. Primer: Searching for efficient transformers for language modeling. In *NeurIPS*, 2021.
- [48] Anand Subramanian. torch_cka. <https://github.com/AntixK/PyTorch-Model-Compare>, 2021.
- [49] Christian Szegedy, Vincent Vanhoucke, Sergey Ioffe, Jon Shlens, and Zbigniew Wojna. Rethinking the inception architecture for computer vision. In *CVPR*, pages 2818–2826, 2016.
- [50] Yuki Tatsunami and Masato Taki. Sequencer: Deep lstm for image classification. In *NeurIPS*, 2022.
- [51] Yi Tay, Dara Bahri, Donald Metzler, Da-Cheng Juan, Zhe Zhao, and Che Zheng. Synthesizer: Rethinking self-attention for transformer models. In *ICML*, pages 10183–10192. PMLR, 2021.
- [52] Ilya O Tolstikhin, Neil Houlsby, Alexander Kolesnikov, Lucas Beyer, Xiaohua Zhai, Thomas Unterthiner, Jessica Yung, Andreas Steiner, Daniel Keysers, Jakob Uszkoreit, et al. Mlp-mixer: An all-mlp architecture for vision. In *NeurIPS*, volume 34, 2021.
- [53] Hugo Touvron, Matthieu Cord, Matthijs Douze, Francisco Massa, Alexandre Sablayrolles, and Hervé Jégou. Training data-efficient image transformers & distillation through attention. In *ICML*, 2021.
- [54] Hugo Touvron, Matthieu Cord, Alexandre Sablayrolles, Gabriel Synnaeve, and Hervé Jégou. Going deeper with image transformers. In *ICCV*, pages 32–42, 2021.
- [55] Shikhar Tuli, Ishita Dasgupta, Erin Grant, and Thomas L Griffiths. Are convolutional neural networks or transformers more like human vision? In *CogSci*, 2021.
- [56] Ashish Vaswani, Noam Shazeer, Niki Parmar, Jakob Uszkoreit, Llion Jones, Aidan N Gomez, Łukasz Kaiser, and Illia Polosukhin. Attention is all you need. In *NeurIPS*, volume 30, 2017.
- [57] Xuan-Thuy Vo, Duy-Linh Nguyen, Adri Priadana, and Kang-Hyun Jo. Dynamic circular convolution for image classification.
- [58] Wenhao Wang, Enze Xie, Xiang Li, Deng-Ping Fan, Kaitao Song, Ding Liang, Tong Lu, Ping Luo, and Ling Shao. Pyramid vision transformer: A versatile backbone for dense prediction without convolutions. In *ICCV*, 2021.
- [59] Ziyu Wang, Wenhao Jiang, Yiming M Zhu, Li Yuan, Yibing Song, and Wei Liu. Dynamixer: a vision mlp architecture with dynamic mixing. In *ICML*, pages 22691–22701. PMLR, 2022.
- [60] Yimin Wei, Hao Liu, Tingting Xie, Qiuhong Ke, and Yulan Guo. Spatial-temporal transformer for 3d point cloud sequences. In *WACV*, pages 1171–1180, 2022.
- [61] Ross Wightman. Pytorch image models. <https://github.com/rwightman/pytorch-image-models>, 2019.
- [62] Ross Wightman, Hugo Touvron, and Hervé Jégou. Resnet strikes back: An improved training procedure in timm. *arXiv preprint arXiv:2110.00476*, 2021.
- [63] Saining Xie, Ross Girshick, Piotr Dollár, Zhuowen Tu, and Kaiming He. Aggregated residual transformations for deep neural networks. In *CVPR*, pages 1492–1500, 2017.
- [64] Brandon Yang, Gabriel Bender, Quoc V Le, and Jiquan Ngiam. Condconv: Conditionally parameterized convolutions for efficient inference. In *NeurIPS*, volume 32, 2019.

- [65] Weihao Yu, Mi Luo, Pan Zhou, Chenyang Si, Yichen Zhou, Xinchao Wang, Jiashi Feng, and Shuicheng Yan. Metaformer is actually what you need for vision. In *CVPR*, 2022.
- [66] Weihao Yu, Chenyang Si, Pan Zhou, Mi Luo, Yichen Zhou, Jiashi Feng, Shuicheng Yan, and Xinchao Wang. Metaformer baselines for vision. *arXiv preprint arXiv:2210.13452*, 2022.
- [67] Li Yuan, Yunpeng Chen, Tao Wang, Weihao Yu, Yujun Shi, Zi-Hang Jiang, Francis EH Tay, Jiashi Feng, and Shuicheng Yan. Tokens-to-token vit: Training vision transformers from scratch on imagenet. In *ICCV*, pages 558–567, 2021.
- [68] Sangdoo Yun, Dongyoon Han, Seong Joon Oh, Sanghyuk Chun, Junsuk Choe, and Youngjoon Yoo. Cutmix: Regularization strategy to train strong classifiers with localizable features. In *ICCV*, pages 6023–6032, 2019.
- [69] Hongyi Zhang, Moustapha Cisse, Yann N Dauphin, and David Lopez-Paz. mixup: Beyond empirical risk minimization. In *ICLR*, 2018.
- [70] Pengchuan Zhang, Xiyang Dai, Jianwei Yang, Bin Xiao, Lu Yuan, Lei Zhang, and Jianfeng Gao. Multi-scale vision long-former: A new vision transformer for high-resolution image encoding. In *Proceedings of the IEEE/CVF International Conference on Computer Vision*, pages 2998–3008, 2021.
- [71] Hengshuang Zhao, Li Jiang, Jiaya Jia, Philip HS Torr, and Vladlen Koltun. Point transformer. In *ICCV*, pages 16259–16268, 2021.
- [72] Zhun Zhong, Liang Zheng, Guoliang Kang, Shaozi Li, and Yi Yang. Random erasing data augmentation. In *AAAI*, volume 34, pages 13001–13008, 2020.
- [73] Bolei Zhou, Hang Zhao, Xavier Puig, Sanja Fidler, Adela Barriuso, and Antonio Torralba. Scene parsing through ade20k dataset. In *CVPR*, pages 633–641, 2017.
- [74] Daquan Zhou, Yujun Shi, Bingyi Kang, Weihao Yu, Zihang Jiang, Yuan Li, Xiaojie Jin, Qibin Hou, and Jiashi Feng. Refiner: Refining self-attention for vision transformers. *arXiv preprint arXiv:2106.03714*, 2021.

A. Detailed information

A.1. Code for Dynamic Filter

The propose dynamic filter can implement briefly by `PyTorch` [40]. Algorithm 1 shows the pseudocode for crucial parts of the dynamic filter.

A.2. Code for Visualization

We utilized Algorithm 2 to visualize the complex parameters on the frequency domain in the global filter and dynamic filter.

A.3. ImageNet-1K Training Setting

We provide ImageNet-1K training settings in Table 6. These settings are used in the main results.

A.4. Replacement of Filters in Ablation

In the ablation study, we replaced dynamic filters with global filters and AFNOs. Here, we describe how to replace them. When replaced by global filters, \mathcal{L} is defined as follows:

$$\mathcal{L}(\cdot) = \mathcal{G}(\cdot). \quad (8)$$

If replaced by AFNOs,

$$\mathcal{L}(\cdot) = \text{AFNO}(\cdot). \quad (9)$$

Training config.	DFFormer- & CDFFormer-S18/S36/M36/B36
dataset	ImageNet-1K [27]
resolution	224 ²
optimizer	AdamW [35]
base learning rate	1e-3
weight decay	0.05
optimizer ϵ	1e-8
optimizer momentum	$\beta_1 = 0.9, \beta_2 = 0.999$
batch size	1024
training epochs	300
learning rate schedule	cosine decay
lower learning rate bound	1e-6
warmup epochs	20
warmup schedule	linear
warmup learning rate	1e-6
cooldown epochs	10
crop ratio	1.0
RandAugment [12]	(9, 0.5)
Mixup α [69]	0.8
CutMix α [68]	1.0
random erasing [72]	0.25
label smoothing [49]	0.1
stochastic depth [24]	0.2/0.3/0.4/0.6
LayerScale [54] init.	None
ResScale [46] init.	1.0 (only for the last two stages)

Table 6: Hyper-parameters of classification on ImageNet-1K

A.5. Detail of Advantages at Higher Resolutions

We discussed the changes in throughput and peak memory during inference when varying the resolution. In the main text, the original measurements of the plotted results are listed in Table 7.

B. More Analysis

B.1. More Visualization of Dynamic Filter Basis

Visualization of the dynamic filter basis in models which we do not mention in the main text, is shown in Figure 11, 12.

B.2. More Models vs Human on Shape Bias

A brief review of previous studies on shape bias shows that FFT-based token-mixers are expected to have more intense shape bias than not global token-mixers. In earlier studies, [2], CNNs are known to be insensitive to global shape information and instead demonstrate a strong reaction to a texture. Later, [23] point out that several data augmentations reduce texture bias and [55] that Transformers have more substantial shape bias than CNN. [14] found that even CNNs can improve the shape bias due to a larger kernel size. Since the FFT-based model performs operations equivalent to those of a large kernel CNN, we expected that the FFT-based model would have a similar trend to CNNs with large kernels about shape bias, and we obtained such results on S18 scale models.

We already have discussed shape bias on S18 scale models, but similarly for other scales. Figure 13 shows them of other scale models. The results tend to be the same as on S18 scale models.

Algorithm 1 Pseudocode for dynamic filter (PyTorch-like)

```
class DynamicFilter(nn.Module):
    def __init__(self, dim, expansion_ratio=2, bias=False, num_filters=4, size=14, **kwargs):
        super().__init__()
        size = to_2tuple(size)
        self.size = size[0]
        self.filter_size = size[1] // 2 + 1
        self.num_filters = num_filters
        self.dim = dim
        self.med_channels = int(expansion_ratio * dim)
        self.pwconv1 = nn.Linear(dim, self.med_channels, bias=bias)
        self.act = StarReLU()
        self.reweight = Mlp(dim, .25, num_filters * self.med_channels)
        self.complex_weights = nn.Parameter(
            torch.randn(self.size, self.filter_size, num_filters, 2,
                        dtype=torch.float32) * 0.02)
        self.pwconv2 = nn.Linear(self.med_channels, dim, bias=bias)

    def forward(self, x):
        B, H, W, _ = x.shape

        routeing = self.reweight(x.mean(dim=(1, 2))).view(B, self.num_filters, -1).softmax(dim=1)
        x = self.pwconv1(x)
        x = self.act(x)
        x = x.to(torch.float32)
        x = torch.fft.rfft2(x, dim=(1, 2), norm='ortho')
        complex_weights = torch.view_as_complex(self.complex_weights)
        routeing = routeing.to(torch.complex64)
        weight = torch.einsum('bfc,hwf->bhwc', routeing, complex_weights)
        weight = weight.view(-1, self.size, self.filter_size, self.med_channels)
        x = x * weight
        x = torch.fft.irfft2(x, s=(H, W), dim=(1, 2), norm='ortho')
        x = self.pwconv2(x)
        return x

class Mlp(nn.Module):
    def __init__(self, dim, mlp_ratio, out_features=None, bias=False, **kwargs):
        super().__init__()
        in_features = dim
        out_features = out_features or in_features
        hidden_features = int(mlp_ratio * in_features)

        self.fc1 = nn.Linear(in_features, hidden_features, bias=bias)
        self.act = StarReLU()
        self.fc2 = nn.Linear(hidden_features, out_features, bias=bias)

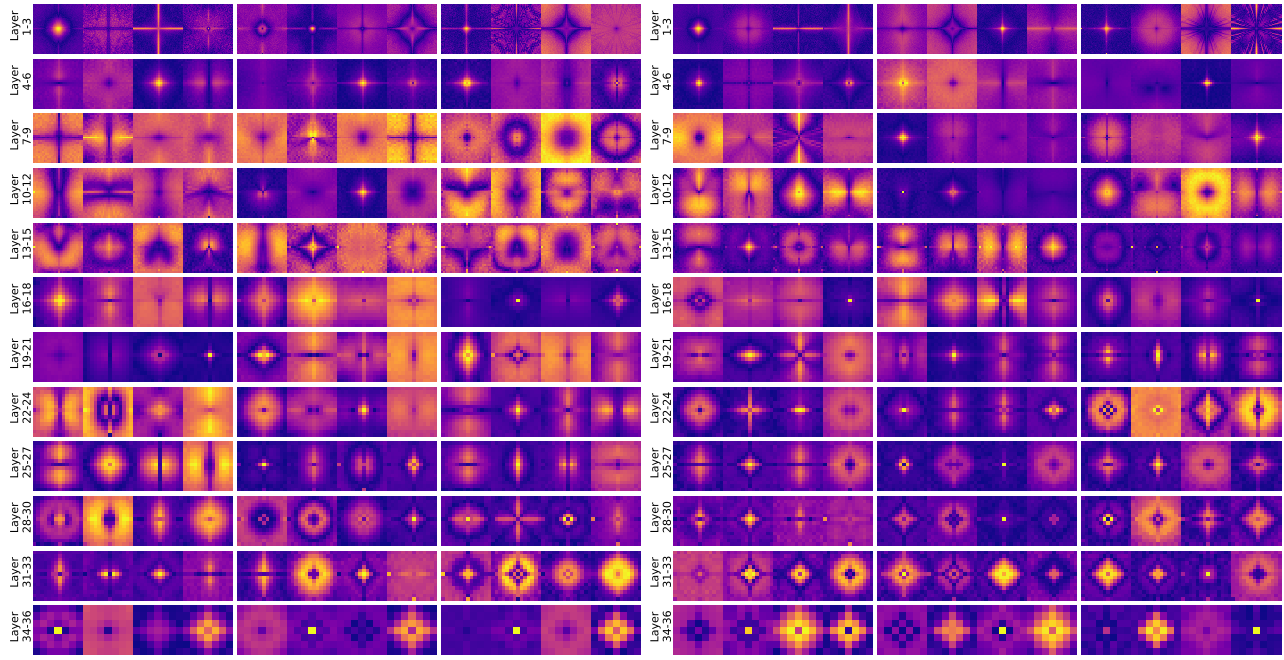
    def forward(self, x):
        x = self.fc1(x)
        x = self.act(x)
        x = self.fc2(x)
        return x
```

Algorithm 2 Pseudocode of visualization of weights in global and dynamic filters (PyTorch-like)

```
def visualize(weight):
    # weight.shape: (height, width, number_of_filter, 2)
    # weight.dtype: torch.float
    weight = torch.view_as_complex(weight)
    amplitude = weight.abs() + 1e-6
    amplitude = amplitude.log()
    amplitude = amplitude.sigmoid()
    h, w, _ = amplitude.shape
    if h % 2 == 0:
        amplitude = torch.cat([amplitude, torch.flip(amplitude[:, 1:-1], dims=[1])], dim=1)
    else:
        amplitude = torch.cat([amplitude, torch.flip(amplitude[:, 1:], dims=[1])], dim=1)
    h, w, _ = amplitude.shape
    amplitude = torch.roll(amplitude, shifts=(int(h / 2), int(w / 2)), dims=(0, 1))
    return amplitude
```

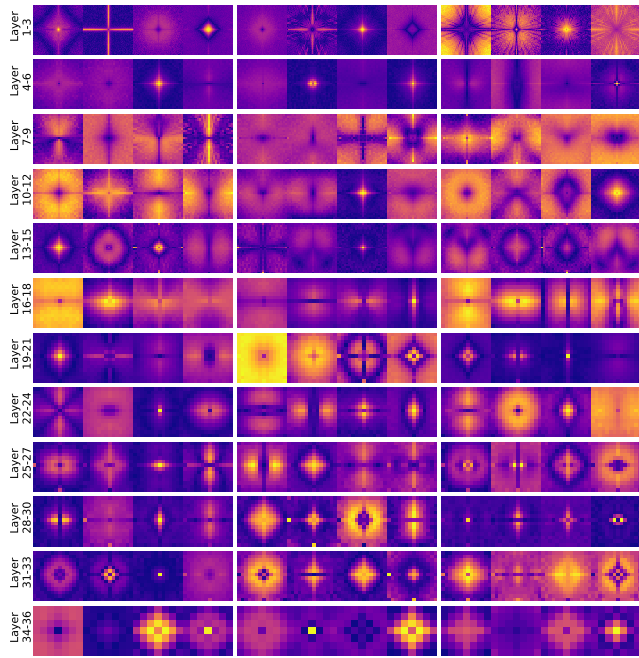
Size	Model\Resolution	Throughput(images/s)				Peak memory (MB)			
		256 ²	512 ²	768 ²	1024 ²	256 ²	512 ²	768 ²	1024 ²
S18	ConvFormer	199.88	149.70	73.25	42.26	171	371	707	1175
	CAFormer	202.64	113.31	35.91	15.61	169	407	1435	4131
	DFFormer	148.59	111.81	54.45	30.54	183	385	723	1192
	CDFFormer	168.99	129.86	63.60	36.97	183	384	720	1188
S36	ConvFormer	107.43	78.95	38.66	22.51	232	421	757	1225
	CAFormer	109.14	59.07	18.53	8.08	229	481	1509	4205
	DFFormer	76.18	58.46	28.55	16.39	265	444	782	1254
	CDFFormer	90.67	68.48	33.73	19.70	263	441	778	1246
M36	ConvFormer	115.30	58.67	28.31	16.33	351	620	1116	1808
	CAFormer	108.48	45.38	14.53	6.43	340	625	1856	5088
	DFFormer	77.51	43.67	20.89	11.69	397	653	1151	1846
	CDFFormer	87.58	51.87	24.95	14.58	393	648	1145	1837
B36	ConvFormer	111.39	43.84	21.16	12.13	577	907	1563	2479
	CAFormer	106.96	33.60	10.89	4.79	583	960	2592	6895
	DFFormer	77.90	33.03	15.85	8.71	663	966	1624	2545
	CDFFormer	86.22	39.03	18.93	10.89	655	959	1615	2531

Table 7: **Throughput vs. resolution and peak memory vs. resolution** these have been benchmarked on a V100 with 16GB memory at a batch size of four. In this paper, we propose the models highlighted with pink as shown are proposed in this paper.



(a) DFFormer-S36

(c) DFFormer-B36



(b) DFFormer-M36

Figure 11: Visualization of dynamic filter basis in the frequency domain on DFFormers

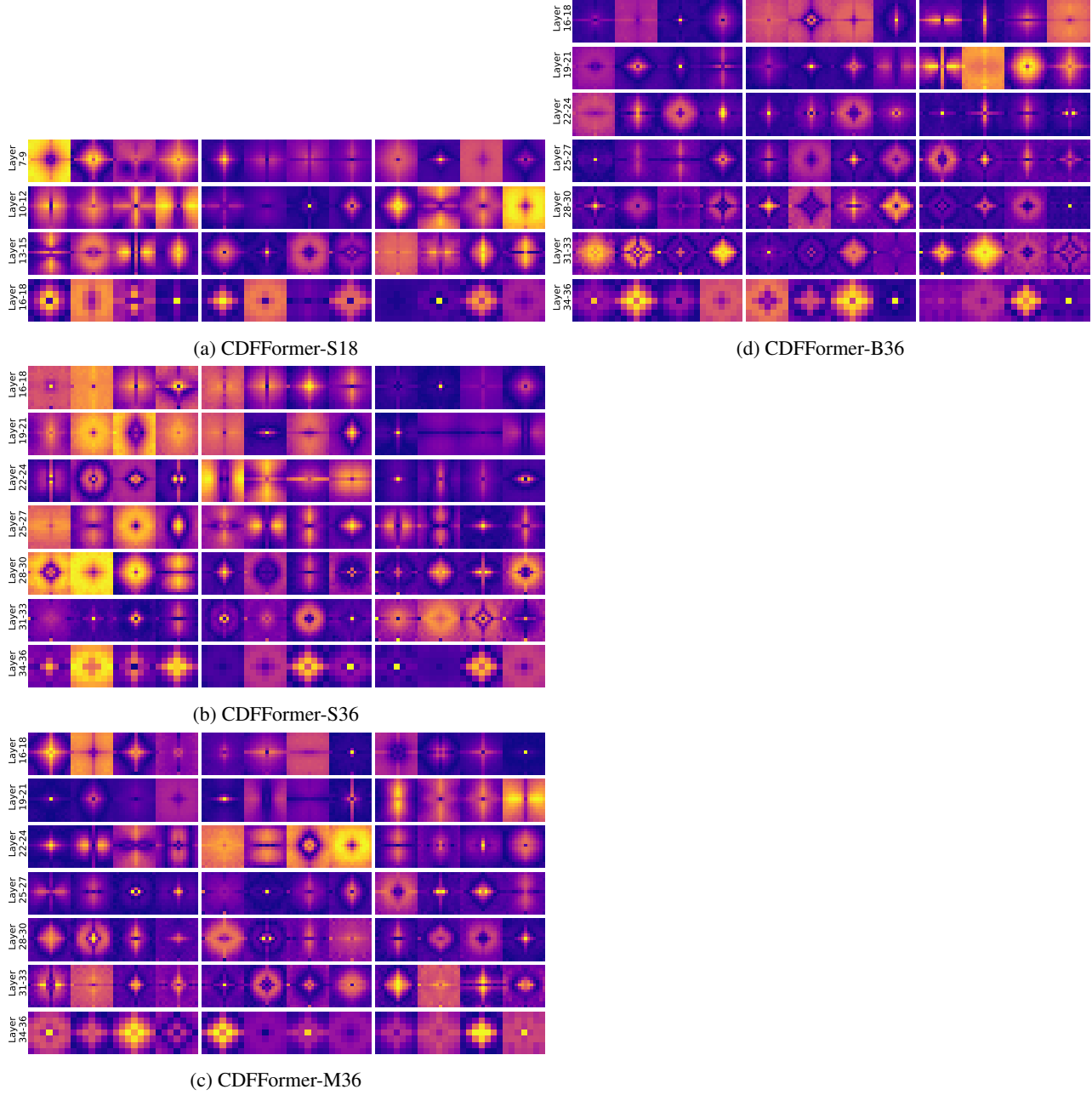
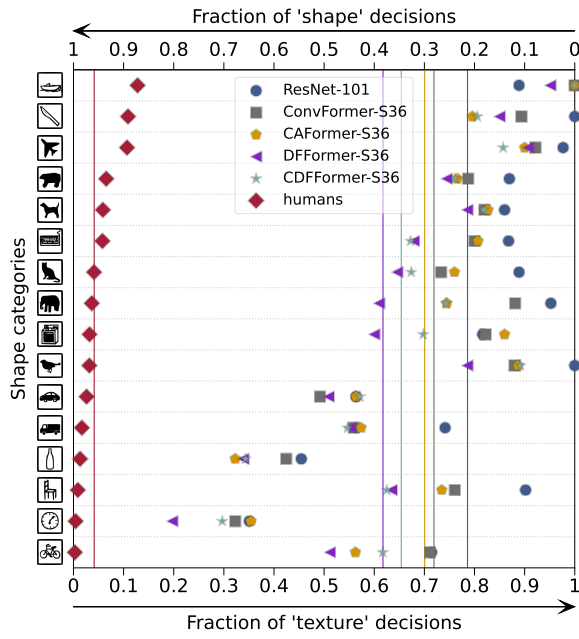
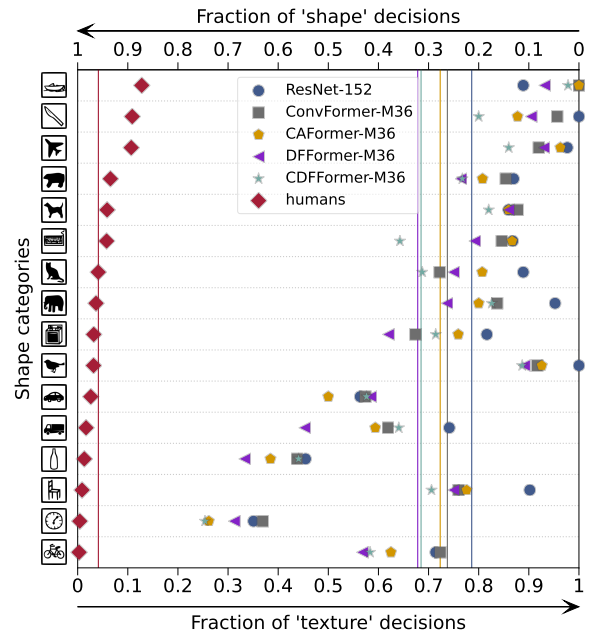


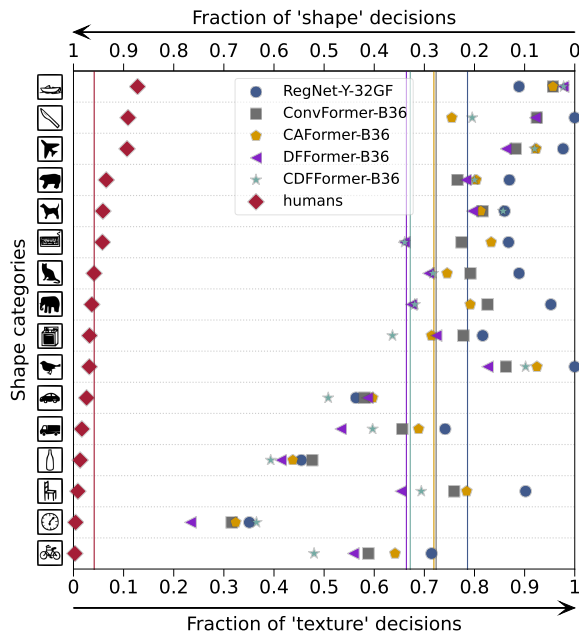
Figure 12: Visualization of dynamic filter basis in the frequency domain on CDFFormers



(a) S36 models vs human on shape bias



(b) M36 models vs human on shape bias



(c) B36 models vs human on shape bias

Figure 13: More shape bias